

## RESEARCH ARTICLE

# Carbon-Cobalt Nanostructures as an Efficient Adsorbent of Malachite Green

Hassan H. Hammud<sup>1\*</sup>, Bassem El Hamaoui<sup>2\*\*</sup>, Nada H. Noubani<sup>3</sup>, Xingliang Feng<sup>4</sup>, Zhong-Shuai Wu<sup>5</sup>, Klaus Müllen<sup>5</sup> and Khurshid Ayub<sup>6</sup>

<sup>1</sup>King Faisal University, Faculty of Science, Chemistry Department, Al-Ahsa 31982, Saudi Arabia; <sup>2</sup>Lebanese University, Chemistry Department, Lebanon; <sup>3</sup>Beirut Arab University, Chemistry Department, Lebanon; <sup>4</sup>Department of Chemistry and Food Chemistry, Technische Universität Dresden, 01062 Dresden, Germany; <sup>5</sup>Max-Planck-Institute for Polymer Research, Ackermannweg 10, D-55122, Mainz, Germany; <sup>6</sup>Department of chemistry, COMSATS institute of information technology Abbottabad, KPK, Pakistan 22060

**Abstract:** Carbon-cobalt nanostructures **1** and **2** were prepared by pyrolysis of the cis-dichlorobis(1,10-phenanthroline-N,N')-cobalt(II) complex **3** in the absence or presence of anthracene respectively. DFT calculation was used to estimate ligand dissociation energy of cobalt complex, the energy cost for the formation of cobalt particles which catalyze the formation of carbon nanostructures. FE-SEM analysis indicates that **1** and **2** contain 3D nanostructure hierarchical porous graphitic carbons HPCGs wrapping cobalt particles in spheres and rods, with mesopores and macropores ranging from 10-100 nm.

---

## ARTICLE HISTORY

Received: November 01, 2016  
Revised: April 02, 2017  
Accepted: April 07, 2017

DOI:  
10.2174/2210681207666170509145222

TEM analysis indicated that nanostructures **1** and **2** consist of graphite layers as well as single wall and bamboo multiple wall carbon nanotubes. Crystalline cobalt catalyst nanoparticles were found wrapped in ordered graphene layers and also at the tips of the bamboo-shaped disordered multi-wall carbon nanotubes. TEM also showed porous surfaces. Both nanostructures **1** and **2** were used as adsorbents to uptake malachite green dye (MG) from aqueous solution. Adsorption isotherms of MG by adsorbents **1** and **2** were fitted in terms of Langmuir, Freundlich, Temkin, and D-R models. The adsorption capacity of **2** (492 mg/g) was higher than that of **1** (200 mg/g). Thermodynamic adsorption studies indicated that the sorption process was spontaneous and exothermic. A pseudo-first order model has been adopted to describe the kinetics of the adsorption process as well as the activated thermodynamic parameters. Column kinetic adsorption of MG by **2** was best fitted by the Thomas model. The column capacity was found to be 64 mg. The adsorbent can be regenerated and proved efficient for three consecutive cycles.

**Keywords:** Carbon nanostructure, cobalt complex, complexation energy, malachite green, adsorption isotherm, thermodynamics, kinetic, column.

## 1. INTRODUCTION

There has been a great interest in the synthesis and characterization of carbon nano structures encapsulating metal nanoparticles due to their various applications in information storage media and as catalysts in the field of medicinal chemistry [1, 2]. Carbon-coated metal nanostructures were prepared by arc discharge processes [3] and solid pyrolysis of surfactant-wrapped metal particles [4]. In the last decade, the solid-state pyrolysis (SSP) of organometallic complexes has been developed as a challenging method towards preparation of carbon-metal nanostructures. However, mixtures of

products were obtained: metal particles with carbon nanotubes CNTs, carbon onions and graphite [5, 6]. Hollow structure with graphitic shells, carbon nanocages CNCs, were obtained from thermolysis of acetylene with iron carbonyl [7]. In addition, the pyrolysis of ferrocene under a flow of argon gas in presence or absence of a hydrocarbon source lead to carbon nanotubes [8], while SSP of iron(II) gluconate afforded graphitic nanopipes and capsules [9]. Remarkably enough, SSP of polyphenylene dendrimer/cobalt complexes produced carbon nanotubes CNTs, uniform carbon cobalt nanorods, and carbon/cobalt nanospheres depending on precursors structures and heating methods (heating temperatures and rates) and that CNTs could be grown from the surface of nanorods and nanosphere by further heating [10]. SSP of Co-carbonyl dehydro[n]anulenes afforded graphitic carbon onions and tubes [11]. Pyrolysis of various organometallic

---

\*Address correspondence to this author at the King Faisal University, Faculty of Science, Chemistry Department, Al-Ahsa 31982, Saudi Arabia; E-mail: [hhammoud@kfu.edu.sa](mailto:hhammoud@kfu.edu.sa); [bassemelhamaoui@gmail.com](mailto:bassemelhamaoui@gmail.com)

complexes in a sealed vessel produces carbon nanocables [12].

However, a great challenge has been focused on the selective production of only one type of nanostructures: Pyrolysis of diphenylacetylene-Cobalt complex afforded CNT's in high yield [5]. SSP of Fe and Co phthalocyanine gave straight and kinked CNT respectively [12]. Thermolysis of hexa-peri-hexabenzocoronenes produced bamboo shaped or straight chain multi wall carbon nanotubes MCNT's depending on the heating process [13]. While SSP of the metal organic framework  $[\text{Ni}_3(\text{btc})_2 \cdot 12\text{H}_2\text{O}]$ , (btc = benzene-1,3,5-tricarboxylato), afforded MCNT's in 65% yield [14].

While SSP of Co-carbonyl complexes of phenyl-alkynes gave carbon Co nanorods or nanospheres depending on the heating temperatures and precursor structures. SSP of Co-carbonyl complexes of graphene-alkyne complex always afforded MCNT's due to the presence of large aryl group graphene [15].

Various refineries as well as chemical and food industries discharge waste water [16]. This waste water often contains colorant residues which may cause several hazards. Such colorant pollutants such as Malachite Green are often toxic and non-biodegradable. Furthermore, optical absorption by dyes or pigments weakens penetration of sun light into water, thus affecting the growth of bacteria and aquatic biota [16].

Common methods for removing colorants from waste water include electrochemical treatment, coagulation, flocculation, chemical oxidation, and adsorption. Adsorption has been found to be an efficient way for removal of organic matter from polluted water in terms of low cost, simple design, and easy operation [17]. Recently, carbon nanostructures have proven high adsorption capacity for cationic dyes and heavy metals such as lead [18], mercury [19], and cadmium [20] due to their great specific surface area and porosity [21].

Herein, we demonstrate the preparation of carbon-cobalt nanostructures **1** and **2** by temperature and pressure controlled solid state pyrolysis of the cis-dichlorobis(1,10-phenanthroline-N,N')-cobalt(II) complex **3**, since it was known that nanoscale metal particles catalyze graphitic carbon formation at high temperatures in the presence of an organic carbon source [22]. The main objective of the present work is to determine the adsorption capacity of cationic dye Malachite Green (MG) by nanostructures **1** and **2** using batch and column experiments. The optimum conditions of contact time, pH, and adsorbent mass will be determined and adopted. Furthermore, kinetic and equilibrium models will be used to fit the experimental results. Adsorption thermodynamic parameters will be also determined.

## 2. EXPERIMENTAL

### 2.1. Preparation of Cobalt-Carbon Nanostructure Adsorbents

*Preparation of starting materials complex 3, cis-[Co(phen)<sub>2</sub>Cl<sub>2</sub>].1.5 acetonitrile:*  $\text{CoCl}_2 \cdot 6\text{H}_2\text{O}$  (0.70 g,  $2.94 \times 10^{-3}$  moles) was dissolved in 40 ml of acetonitrile. Phe-

nanthroline monohydrate (0.265 g,  $1.47 \times 10^{-3}$  moles) was then added. The mixture was heated for two hours and the product **3** was precipitated after two days. Filtration and drying resulted in 50% yield. Crystals of **3** can be also prepared [23].

*X-Ray analysis:* Single red square crystals of *cis-[Co(phen)<sub>2</sub>Cl<sub>2</sub>]. DMF 4* were obtained by re-crystallization of the precipitate **3** in DMF/acetonitrile, its crystal structure was analyzed by X-ray diffraction was characterized by a Bruker D4 X-ray scattering systems with Ni-filtered  $\text{Cu K}\alpha$  radiation. It was found similar to the one reported in [23], and has the same unit structure *cis-[Co(phen)<sub>2</sub>Cl<sub>2</sub>]*.

*Computational methodology:* DFT calculations were performed through the Gaussian 09 suite of programs [24]. A number of pure and hybrid functionals along with different combinations of basis sets have been evaluated for the theoretical simulations of geometries of Co complex. The geometries are optimized without any symmetry constraints. This complex was confirmed as true minima on potential energy surface (PES) through frequency analysis (no imaginary frequency) at the same level of theory. To determine the stability of the complex unit *cis-[Co(phen)<sub>2</sub>Cl<sub>2</sub>]*, binding energies of ligands with cobalt metal were calculated through geometrical counterpoise corrected energy ( $\Delta E_{\text{gCP-D3}}$ ) simulations [24]. The optimized geometries are plotted through GaussView (Version 5, 2009).

*Preparation of carbon-cobalt nanostructure adsorbent 1:* Adsorbent **1** consists of carbon-cobalt nanostructures obtained by pyrolysis of complex **3** under low nitrogen pressure in a vacuum-inert atmosphere furnace (KJ-1200G) at 600 °C for five hours [10, 13].

*Preparation of carbon-cobalt nanostructure adsorbent 2:* Complex **3** was grinded and mixed with anthracene ( $\text{C}_{14}\text{H}_{10}$ ) (1:1) and then pyrolyzed under vacuum in a vacuum-inert atmosphere furnace under reduced nitrogen pressure for five hours at 600 °C to produce carbon-cobalt nanostructures, adsorbent **2** [15, 25].

### 2.2. Adsorbate Stock Solution

The cationic dye MG ( $\text{C}_{23}\text{H}_{26}\text{N}_2\text{O} \cdot \text{HCl}$ , 85%,  $\lambda = 618$  nm,) was supplied by Sigma Aldrich. All working standard solutions used in the experiments were prepared by properly diluting the stock solution (1000 mg/L) with deionized water.

### 2.3. Characterization of Adsorbents

*Thermal Analysis:* Thermogravimetric – Differential Thermal Analysis (TG-DTA) curves were measured on SETARAM LABSYS Thermal analyzer in the flow of  $\text{N}_2$  gas, within the 20-700 °C temperature range, with a rate of heating 3°C/min [26-28].

*Field Emission Electron Microscope analysis:* FE-SEM images were measured by JSM 7600F, Jeol instrument, Japan.

*Transmission Electron Microscope TEM analysis:* TEM and high resolution HRTEM images was measured by a Philips Tecnai F20 instrument.

## 2.4. Adsorption Agitation Batch Study

The adsorption measurements were determined by adding and shaking the required amount of adsorbent 0.01 g with 10 ml of aqueous Malachite Green MG solutions of known concentrations in a series of 50 ml volumetric flasks. The solutions were shaken at constant agitation speed (160 rpm) with a shaker incubator (SHIN SAEN6, SKIR-601 MODEL) for a fixed period of contact time. After the requested time, suspensions were analyzed for residual MG concentrations by measuring absorbance at  $\lambda_{\max} = 618$  nm and applying calibration curve techniques. The absorbance was measured with a UV-visible spectrophotometer (SP-3000 Plus Optima, Tokyo Japan). Adsorption experiments were carried by changing the initial dye concentration, pH, contact time and temperature. The obtained optimum conditions were adopted in the adsorption kinetics, isotherms, and thermodynamic studies.

The uptake of malachite green by the adsorbents **1** and **2**,  $q_t$  (mg/g) at time  $t$  (min) was calculated using the mass balance equation:

$$q_t = (C_0 - C_e) \frac{V}{m} \quad (1)$$

where,  $C_0$  and  $C_e$  (mg/l) are the original and equilibrium dye concentrations, respectively,  $V$ (l) is the solution volume and  $m$ (g) is the adsorbent weight.

*Effect of pH:* In order to study the effect of pH on malachite green adsorption, 10 mg of **2** was added to solutions containing 10 ml of 200 mg/l of MG. The initial pH values were adjusted from 2-10 using 0.1M HCl or 0.1M NaOH solutions. After suspensions had been shaken for 24 hours at 25 °C, the absorbance of solutions were measured for residual MG concentration.

## 2.5. Kinetic Adsorption Studies

For kinetic studies, 10 ml of 200 mg/l of malachite green dye was treated with 10 mg of adsorbents **1** or **2** at various temperatures (298, 303, 308, and 313 K) in a shaker incubator. The working pH of the solution was 7.0. Aliquots were analyzed for the remaining MG at 15 min intervals.

## 2.6. Adsorption Isotherms

10 mg of **1** or **2** was used to treat 10 ml solution of 10 - 1000 mg/l of dye, respectively. The mixtures were agitated in a shaker incubator continuously for 4 hours to reach equilibrium, at various temperatures (298, 303, 308, and 313 K). Suspensions were then analyzed for residual MG concentrations.

## 2.7. Column Adsorption Study

Fixed-bed column studies were carried out using a column having 2 cm inner diameter and loaded with 0.5 g of adsorbent **2**. Malachite green solution of initial concentration 200 mg/L was then added to the column with a flow rate of 2 mL/min. The effluent samples were collected at specified intervals of time, and their absorbance were measured for determination of residual MG concentration. Elution was stopped when the column became exhausted. The saturation

point of the first cycle was reached after passage of 320 ml of MG (200 ppm) solution. While for the second cycle and third cycle, saturation is reached after elution of 230 mL of MG. In each cycles a regeneration of the column is made by washing the column with 100 ml of 0.1 M HCl and then with deionized water.

## 3. METHODS

### 3.1. Kinetics Models

Study of adsorption kinetics is based on the change of adsorption capacity with respect to time and provide information on the nature of adsorption mechanisms. The following models are used:

#### a. Pseudo-first Order Model

The adsorption kinetics can be presented by pseudo-first order equation as proposed by Lagergren [29].

$$\log(q_e - q_t) = \log q_e - \frac{k_1 t}{2.303} \quad (2)$$

Where  $k_1$  ( $\text{min}^{-1}$ ) is the rate constant of the pseudo-first order model. It can be experimentally measured from the slope of the linear plot of  $\log(q_e - q_t)$  versus  $t$  (min).  $q_t$  (mg/g) denotes the amount of adsorption at time  $t$  (min), and  $q_e$  (mg/g) is the amount of adsorption at equilibrium.

#### b. Pseudo-second order model:

The pseudo-second order equation eq. (3) was developed by Ho and McKay, where  $k_2$  (g/mg.min) is the rate constant of the pseudo-second order [30].

$$\frac{t}{q_t} = \frac{1}{k_2 \cdot q_e^2} + \frac{t}{q_e} \quad (3)$$

$k_2$  and  $q_e$  can be measured from the intercept and slope, respectively, of plotting  $t/q_t$  versus  $t$ .

## 3.2. Adsorption Isotherm

Adsorption isotherms explain how adsorbates interact with an adsorbent. Thus the correlation of equilibrium data using either a theoretical or empirical equation is necessary for interpretation and prediction of adsorption process. Four famous linear and nonlinear isotherm equations for Langmuir, Freundlich, Temkin, and Dubinin-Radushkevich (D-R) models, were employed to describe the experimental results of adsorption isotherms, Table 1 [31-33], where  $Q_e$  is the amount of solute adsorbed per unit mass of adsorbent (mg/g), and  $C_e$  is the aqueous phase concentration of the remaining adsorbate at equilibrium (mg/L or ppm) [34-37].

## 3.3. Column Study

The efficiency of a biomass adsorbent and the dynamic behavior of a fixed bed column can be determined from the breakthrough curve, which is the plot of adsorbed dye concentration  $C_{ad}$  as a function of time  $t$  [38]. The total adsorbed MG quantity  $q_{total}$  and the column adsorption capacity  $q_e$  for a given feed concentration  $C_0$ , mass of adsorbent  $m$  and flow rate  $Q$ , can be calculated from the area  $A$  under the breakthrough curve using the equations in Table 2.  $m_{total}$ , the total

**Table 1.** Adsorption isotherm equations of MG onto adsorbents 1 and 2.

	Linear	Non Linear
Langmuir	$\frac{C_s}{Q_s} = \frac{1}{Q^\circ K_L} + \frac{C_s}{Q^\circ}$	$Q_s = \frac{Q^\circ K_L C_s}{1 + K_L C_s}$
Freundlich	$\ln Q_s = \ln K_F + \frac{1}{n} \ln C_e$	$Q_s = K_F (C_s)^{1/n}$
Temkin	$Q_s = B_T \ln K_T + B_T \ln C_s$	$Q_s = B_T \ln(K_T) + B_T \ln(C_s)$
Dubinin-Radushkevich	$\ln Q_s = \ln Q_m + \beta [RT \ln \left(1 + \frac{1}{C_e}\right)]^2$	$Q_s = Q_m \exp^{\beta [RT \ln \left(1 + \frac{1}{C_e}\right)]^2}$

**Table 2.** Column adsorption capacity calculation for MG onto adsorbent 2.

parameter	$A =$	$q_{total} =$	$m_{total} =$	% totalremoval =	$q_s =$	$C_s =$
Equation	$\int_{t=0}^{t=t_{total}} C_{ads} dt$	$\frac{QA}{1000}$	$\frac{C_o Q t_{total}}{1000}$	$\frac{q_{total}}{m_{total}} \times 100$	$\frac{q_{tot}}{m}$	$C_o - \frac{A}{t_{total}}$
unit	mg.min/L	mg	Mg	%	mg/g	mg/L
Cycle 1	15958.3	31.92	58.72	54.36	63.84	83.75
Cycle 2	11329.1	22.66	42.20	53.69	45.32	84.96
Cycle 3	10566.5	21.13	44.96	47.38	42.27	97.27

**Table 3.** Linear equations of different kinetic column models. Column parameters of different models for the first cycle of adsorption of MG onto adsorbent 2.

Thomas model	Linear Equations	Parameters		$R^2$	
	$\ln \left[ \left( \frac{C_o}{C_s} \right) - 1 \right] = \left( \frac{k_{Th} q_T M}{Q} \right) - (k_{Th} C_o t)$	$k_{Th}$ mL.(mg min) <sup>-1</sup>	$q_{Th}$ (mg g <sup>-1</sup> )		0.98
		0.25	60.50		
Yoon-Nelson model	Linear Equations	$k_{YN}$ (min <sup>-1</sup> )	$\tau_{YN}$ (min)	$q_{YN}$ (mg/g)	0.96
	$\ln \left( \frac{C_s}{C_o - C_s} \right) = k_{YN} t - \tau_{YN}$	0.04	90.83	66.67	
Yan's model	Linear Equations	$k_Y$ ml.(mg.min) <sup>-1</sup>	$q_Y$ (mg.g <sup>-1</sup> )		0.90
	$\ln \left[ \left( \frac{C_s}{C_o - C_s} \right) \right] = \left( \frac{k_Y C_o}{Q} \right) \ln \left( \frac{Q^2}{k_Y q_Y m} \right) + \left( \frac{k_Y C_o}{Q} \right) \ln t$	8.95	94.90		

amount of MG dye sent to column, can be also evaluated [36, 37, 39].

Various kinetic models according to Thomas [40], Yoon-Nelson [41] and Yan et al [42] were used to predict the dynamic behavior of the column [34-37]. The experimental column data, equilibrium concentration  $C_e$  (mg/l) versus time  $t$  (min), was fitted to the model equation in order to determine the rate constant  $k$ , maximum capacity of sorption  $q$ , and correlation coefficient  $R^2$ , Table 3.

## 4. RESULTS AND DISCUSSION

### 4.1. Structure of Starting Material Complex 3, cis-[Co(phen)<sub>2</sub>Cl<sub>2</sub>]. 1.5 Acetonitrile

Cobalt (II) ion in complex 3 adopts an octahedral coordination forming bonds with two chloride ions cis to one another, and four nitrogen atoms from two bidentate 1,10-phenanthroline ligands, Fig. (1) [23].

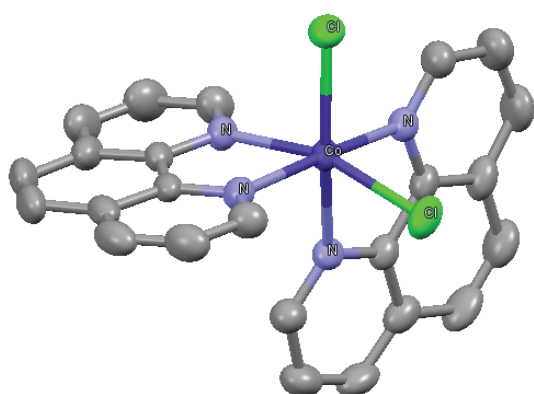
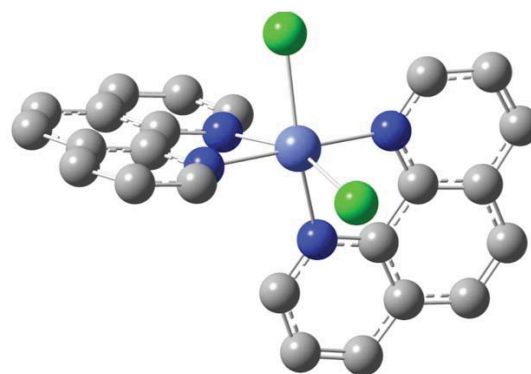


**Fig. (1).** Ellipsoid structure of complex **3**: cis-Cobalt(II) bisphenanthroline dichloride. 1.5 acetonitrile.

## 4.2. Bonds Distances, Complexation Energies, and Relative Energies of the Complex cis-[Co(phen)<sub>2</sub>Cl<sub>2</sub>] in Different States

### 4.2.1. Optimized Geometry of Complex

In the first step towards exploration of the optimized geometry, the complex was optimized in three different multiplicities; doublet, quartet and sextet. The optimized geometric parameters around the cobalt center along with relative energies of the complexes are given in the table 4 below. The quartet spin of the cobalt complex is thermodynamically the most stable spin state. The doublet complex lies 18.12 kcal mol<sup>-1</sup> higher in energy whereas the sextet complex is 44.8 kcal mol<sup>-1</sup> higher in energy. Moreover, the Co-N<sub>1</sub>, Co-N<sub>2</sub> and Co-Cl bond distances for the quartet spin complex agree nicely with the corresponding experimental bond lengths in cis-[Co(phen)<sub>2</sub>Cl<sub>2</sub>]. DMF (4), Table 4.



ple, N2-C2 and N1-C1 bond distances are 1.347 Å and 1.348 Å, respectively which are deviating considerably from the experimental 1.360 Å and 1.361 Å, respectively. The B3LYP and X3LYP methods, on the other hand, can reliably predict the geometric parameters of these complexes in the phenanthroline moiety and in the vicinity of the metal. Higher basis sets are no better than 6-31G(d), rather, relatively poor results are obtained when the diffuse function is included in the calculations. These results suggest that B3LYP/6-31G\* and X3LYP/6-31G\* level of theories are reliable enough to predict the properties of cobalt phenanthroline complexes.

### 4.2.2. Complexation Energies

Since B3LYP/6-31G\* level of theory can reliably predict the properties of these cobalt complexes; therefore, we have calculated the binding energies of these complexes at the same level of theory. The geometric counterpoise correction is then applied to nullify the effects from basis set superposition. Loss of first phenanthroline ligand has thermodynamic cost of 30.97 kcal mol<sup>-1</sup> whereas the loss of 2<sup>nd</sup> phenanthroline ligand requires 60.14 kcal mol<sup>-1</sup>. The higher energetic demand for the loss of the second phenanthroline ligand is

**Table 4.** Comparison of calculated geometries of cobalt complexes in different spin states with the experimental geometric parameters and relative energies of complexes in different spin states. All bond lengths are in Angstroms.

	Co-N <sub>1</sub>	Co-N <sub>2</sub>	Co-Cl	E <sub>relative</sub> (kcal mol <sup>-1</sup> )
Exp	2.151	2.164	2.41	
Doublet	2.188	1.977	2.329	18.12
Quartet	2.176	2.23	2.398	0
Sextet	2.136	2.153	2.272	44.8

Next, a number of pure and hybrid functionals including range separated wB97XD were evaluated in simulating the geometric parameters of the cobalt complex. Comparative analysis of different method in predicting the geometric parameters of the cobalt complex are given in Table S1, ESI. The results illustrate that mPW1PW91 and PBE0 are very good at simulation of Co-N<sub>1</sub>, Co-N<sub>2</sub> and Co-Cl bond distance. For example, the calculated Co-N<sub>1</sub> (2.158 Å) and Co-N<sub>2</sub> bond distance (2.205 Å) correlates nicely with the experimental 2.151 Å and 2.164 Å, respectively. However, these methods are relatively less reliable in properly estimating the C-C bond lengths in the phenanthroline moiety. For exam-

consistent with the literature [43]. The loss of a phenanthroline ligand in the cobalt dichloride complex is relatively more facile than [Co(Phen)<sub>3</sub>]<sup>+2</sup> complex. This difference may be attributed to strong electrostatic interactions in [Co(Phen)<sub>3</sub>]<sup>+2</sup>; however, in the dichloride complex, the charge density on cobalt is decreased due to bonding with chloride

## 4.3. Synthesis and Characterization of Adsorbents

Adsorbent **1** was prepared by heating the cis-cobalt(II) bisphenanthroline dichloride 1.5 acetonitrile (complex **3**) at 600 °C for five hours in an oven, under reduced nitrogen

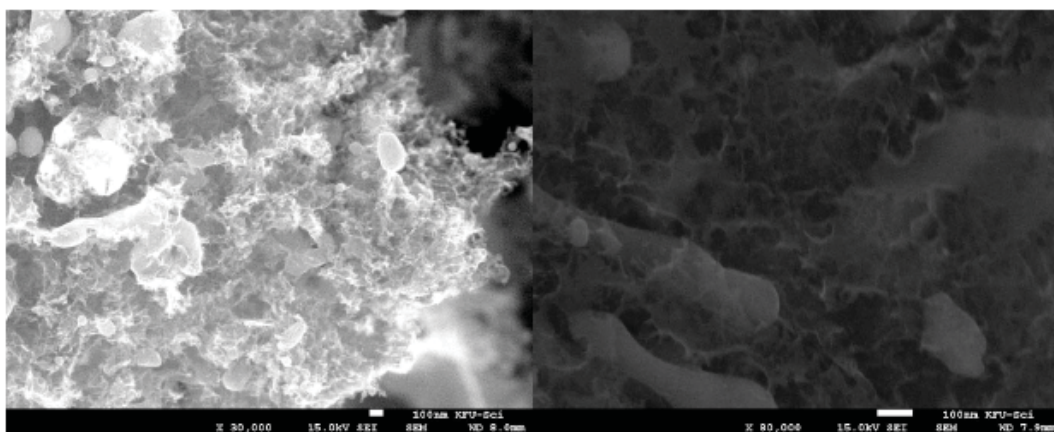


**Fig. (2).** a) FE-SEM images of adsorbents **2** showing 3D nanostructure hierarchical porous graphitic carbons HPCGs wrapping spherical and rod shape cobalt particles. b) Higher magnification FE-SEM top view image of adsorbents **1** indicating the presence of mesopores and macropores ranging from 20-100 nm within HPCGs.

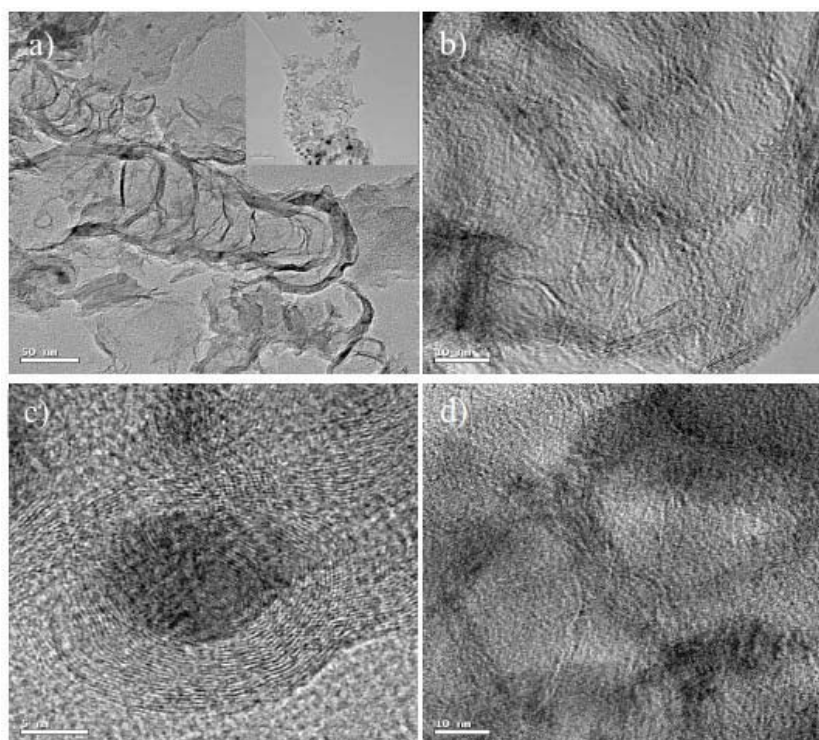


**Fig. (3).** Transmission electron microscopy images of **1** and **2**; a) presence of bamboo-shaped MWCNT's of **1**; b) Presence of ordered arrays of graphite and isolated SWCNT's of **1**. c) Crystalline cobalt nanoparticles surrounded with graphene layers from **2** d) Highly ordered hollow onions from **2**.

pressure. Adsorbent **2** was prepared similarly but with addition of anthracene [13-15, 25]. In the present solid-state pyrolysis, the inorganic complex acts as both catalyst precursor and as carbon source, while anthracene serves as an additional carbon source in the preparation of **2**.

The microstructures of the prepared adsorbents **1** and **2** are similar as indicated by observation with a field emission scanning electron microscopy (FE-SEM). Fig. 2(a) confirms that **2** has 3D carbon architectures with interconnected macroporous frameworks and flake-like carbon walls wrapping white cobalt particles with spherical and rod shapes of varying size of 20 to more than 100 nm [25b]. This proves

the involvement of cobalt particles as catalyst in the formation of 3D nanostructure hierarchical porous graphitic carbons HPCGs. Fig. 2(b) is a higher magnification FE-SEM image of **1**. It further reveals that the 3D HPCGs contains mesopores and macropores ranging from 10-100 nm. The proved porous structure is thus responsible for the adsorption of Malachite Green in water.

The black powders obtained were also analyzed by Transmission Electron Microscopy (TEM). Low and high resolution TEM images of the materials **1** and **2** were displayed in Fig. (3). The TEM micrographs of the respective materials exhibited various aspects of carbon nanostructures.

**Table 5.** Data for thermal analysis of carbon-cobalt nanostructures 1 and 2.

Sample	Temperature Range or Peak (°C) ± 0.01	% Experimental Mass Loss ± 0.03	Enthalpy (J/g) (Process) ± 0.05
(1)	50-175	8.00	-
	175-350	4.50	-
	410.29	11.40	-1930.05 (Exothermic)
	520-700	36.00	-
(2)	50-150	3.90	-
	150-400	2.00	-
	505.90	3.40	993.05 (Endothermic)
	590-700	6.70	-

TEM images of **1** and **2** displayed disordered bamboo-shaped multi wall carbon nanotubes with an average length of several tens nanometers (Fig. **3a** and inset).

However, high-resolution TEM revealed the formation of highly ordered graphitic structures and isolated single-wall carbon nanotubes SWCNT's (Fig. **3b**) unlike a former study from which the pyrolysis of a hexa-*peri*-hexabenzocoronene-cobalt complex at 600 °C even for 8 hours could only afford worm-like nanostructures [13].

Indeed, a high-resolution TEM image (Fig. **3c**) disclosed that the metal carbon nanostructure comprised well-ordered graphene layers (around 22 layers in the wall) surrounding crystalline metal particles (Fig. **3c**). The diameter of the metal nanoparticles varied around 70 nm. This indicates the role of the metal nanoparticles as catalyst towards highly ordered carbon using simple molecules such as anthracene as carbon source. The inter-distance between two graphenic walls was found to be around 0.36 nm, typical for graphitic structures. However, smaller metal particles which catalyzed the synthesis of SWCNTs could not be seen. Fig. (**3d**) shows radial graphene layer structures with no metal particles. Both carbon-cobalt nanostructures **1** and **2** provided similar results by TEM analysis.

One can thus propose the following mechanisms of carbon nanostructure formation. With increasing temperature the complex decomposes, the fragmented ligands also decompose into H<sub>2</sub>, benzene rings and amorphous carbon, the presence of anthracene affords additional biphenyl and benzene rings in the case of **2**. The decomposed gas converts Co<sup>2+</sup> into Co nanoparticles through reduction. The cobalt nanoparticles then act as catalysts for formation of graphite layers from amorphous carbon and benzene according to a dissolution - precipitation mechanism. Spherical cobalt nanoparticles of suitable shape and size can induce the formation of cylindrical graphite layers and consequently carbon nanotubes, as evidenced by the presence of cobalt nanoparticles at the top of bamboo shaped multiple wall carbon nanotubes [14, 15].

In a typical thermal analysis experiment [26-28], carbon-cobalt nanostructures **1** and **2** were heated up to 800 °C under nitrogen where all related weight loss was complete. The percent mass loss and enthalpy change (J/g) at each tempera-

ture peak or range are shown in Table **5**. Both materials were previously carbonized during their preparation by pyrolysis at 600 °C for five hours, and hence their mass loss obtained from thermal analysis is low. **2** is more completely carbonized than **1** for two reasons: first the % residue obtained after thermal analysis for **2** (84%) is greater than for **1** (36%), second an exothermic peak ( $\Delta H = -1930.05$  J/g) was found at 410.29 °C for **1** suggesting that more carbon-carbon bonds can be formed from pyrolysis of **3**. The TG curves decreased continuously above 600 °C because of cobalt volatilization.

#### 4.4. Adsorption of Malachite Green onto Adsorbents 1 and 2 (Batch Experiments)

Carbon nanostructures **1** and **2** were prepared by pyrolysis and characterized, and found to have porous structures consisting of cobalt nanoparticles and graphitic carbon nanostructures containing CNT's as described above were now utilized as adsorbent **1** and **2** respectively in the following adsorption experiments.

##### 4.4.1. Effect of pH of MG Solution on the Adsorption Process

The pH of the dye solution has a great influence on the adsorption capacity. As shown in Fig. (4), a steady increase in adsorption capacity of carbon material was noticed as the

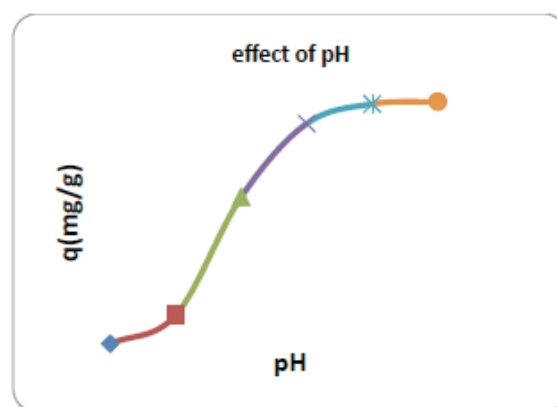


**Fig. (4).** The effect of pH on the adsorption of malachite green onto adsorbent **2**.

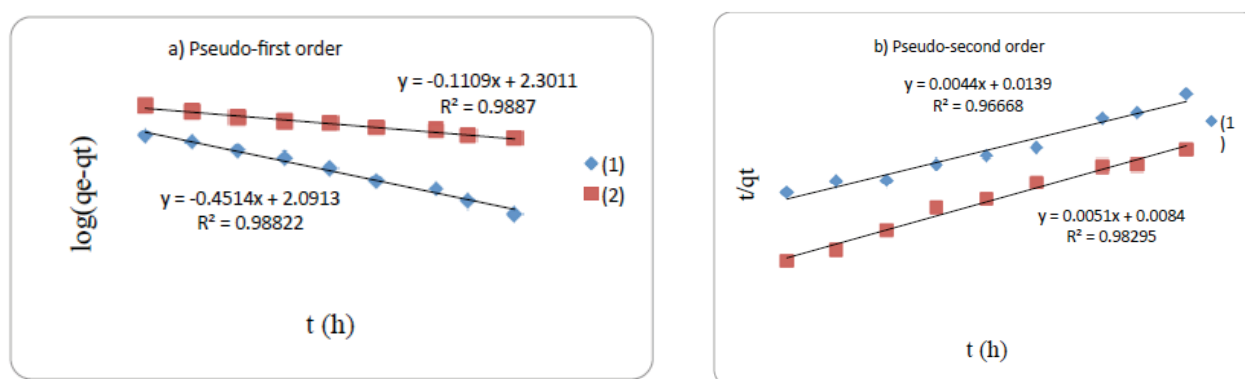


**Fig. (5).** Adsorption kinetic models for adsorption of MG onto adsorbent 1 and 2 at 25 °C: a) Pseudo-first order and b) Pseudo-second order.

pH increased from 2.0 to 6.0. On the other hand, slight capacity increase was observed in the pH range of 6.0 to 12.0. At low pH, the number of negatively charged sites of adsorbent decreased while the number of positively charged surface sites increased. This reduces the adsorption of cationic MG dye due to electrostatic repulsion. Moreover, the lower adsorption of malachite green at acidic pH can be also due to the presence of excess  $H^+$  ions competing with dye cations for the available adsorption sites [37].

#### 4.4.2. Adsorption Kinetics

Two kinetic models, pseudo-first order and pseudo-second order, were used to fit batch experimental adsorption data for the adsorption of malachite green onto adsorbent 1 and 2, the obtained plots are shown in Fig. (5). The kinetic parameters for the adsorption processes were calculated from

these graphs and are presented in Table 6. It is noticed that a pseudo-first order model adequately fits the experimental data of the adsorption process by both nanostructures. In both rate orders the regression parameter  $R^2$  exceeds 0.93 but the  $q$  values calculated from a pseudo first-order model were closer to the experimental  $q$  values than the ones calculated from the pseudo second-order model [35-37, 44].

#### 4.4.3. Adsorption Mechanism

The kinetic results were studied for the adsorption mechanism of MG by adsorbents 1 and 2. Fitting the experimental data in an intra-particle diffusion plot is the most widely used technique for determining the mechanism of the adsorption process. The equation of intra-particle diffusion is:  $q_t = k_i t^{1/2} + I$

**Table 6.** Kinetic parameters and correlation coefficients for the adsorption of MG onto adsorbents 1 and 2.

Sample	Temperature (K)	$q_{exp}$ (mg.g <sup>-1</sup> )	Pseudo-first Order			Pseudo-second Order		
			$q_{calc}$ (mg.g <sup>-1</sup> )	$k_1$ (h <sup>-1</sup> )	$R^2$	$q_{calc}$ (mg.g <sup>-1</sup> )	$k_2$ (g.mg <sup>-1</sup> .h <sup>-1</sup> )	$R^2$
(1)	298	102.16	123.39	1.04	0.99	227.27	0.0013	0.97
	303	157.25	149.01	1.07	0.99	256.41	0.0014	0.95
	308	170.80	158.48	1.13	0.99	270.27	0.0015	0.99
	313	185.93	161.10	1.20	0.97	250.00	0.0039	0.98
(2)	298	189.30	200.03	0.26	0.99	200.00	0.003	0.98
	303	191.49	218.77	0.29	0.97	204.08	0.0025	0.97
	308	192.15	219.28	0.32	0.99	256.41	0.0011	0.99
	313	198.82	228.87	0.38	0.99	263.15	0.0016	0.99

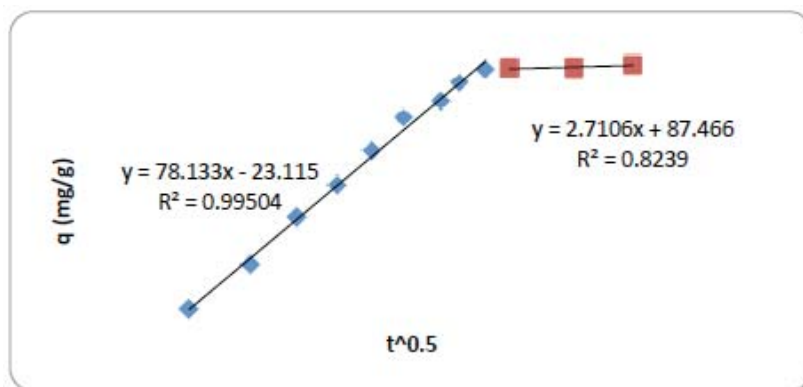


Fig. (6a). Intra-particle diffusion plot for MG adsorption onto adsorbent 1 at 25 °C.

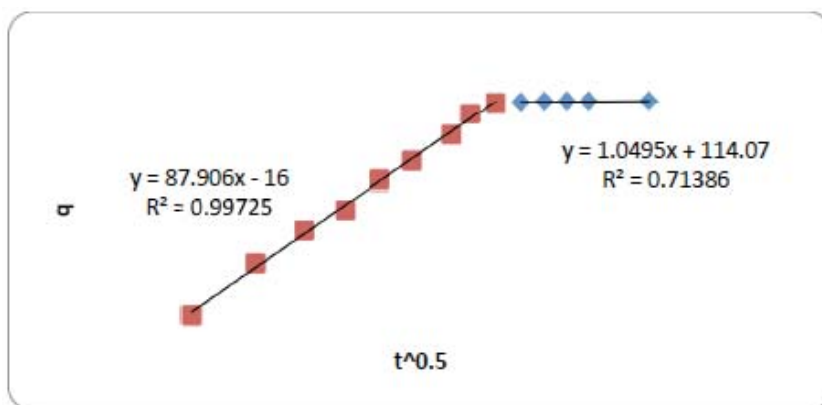


Fig. (6b). Intra-particle diffusion plot for MG dye adsorption onto adsorbent 2 at 25 °C.

where the slope  $k_i$  is the intra-particle diffusion rate constant, and the intercept  $I$  provides information about the thickness of the boundary layer [36, 37].

A multi-stage adsorption is observed in the adsorption of MG onto adsorbents 1 and 2 as is shown in Figs. (6a and 6b). This plots represents two distinct stages; which are external mass transfer followed by intra-particle diffusion, signifying that the dye molecules are transported to the external surface of adsorbent through film diffusion with a high rate. MG molecules were then entered onto adsorbent pores through diffusion. The straight line is not passing through the origin. This indicates that intra-particle diffusion contributes to the adsorption process but is not the only rate determining step [36, 37]. The film diffusion rate constant  $k_{fd}$  ( $\text{mg/g}\cdot\text{hr}^{0.5}$ ) and intra-particle diffusion rate constants  $k_{id}$  ( $\text{mg/g}\cdot\text{hr}^{0.5}$ ) for adsorbent 1 are 78.13 and 2.71 and for adsorbent 2 are 87.91 and 1.05 respectively.

#### 4.4.4. Adsorption Isotherms of MG Onto Adsorbent 1 and 2

The adsorption equilibrium data for MG onto 1 and 2 were analyzed using Langmuir, Freundlich, Temkin and Dubinin-Radushkevich isotherm expressions using linear and non linear models, see Table 1 [31-37]. The resulting capacities, constants and coefficient are presented in Tables 7-10.

The coefficients and parameters of Langmuir and Freundlich isotherms at different temperatures are summarized in Tables 7 (linear model) and 8 (non linear model). Correlation coefficients show that the experimental data are better fitting

a Langmuir than Freundlich isotherm because  $R^2$  of the former is near to unity (Tables 7 and 8), Fig. (7). This indicates a monolayer coverage of malachite green on the outer surface of adsorbent and that adsorption occurs uniformly on the active homogenous adsorption sites. Adsorbent 2 possesses a higher maximum adsorption capacity  $Q^0$  (492.01 mg/g) compared to 1 (200.60 mg/g) because it contains a greater number of active sites on its surface, Table 8.

The values of  $K_L$  “Langmuir coefficient related to sorbent-sorbate affinity” and  $K_F$  “Freundlich capacity factor” for the adsorption of MG on 2 are higher compared to 1 suggesting that the interaction of 2 with MG has a greater binding energy than with 1 (Tables 7 and 8).

$R_L$  being equal to  $1/(1+(C_0\cdot K_L))$  is a characteristic feature of Langmuir isotherm which predicts whether the adsorption is favorable or not [45].  $R_L$  values (Table 7) were smaller than 1 and greater than zero which suggests favorable adsorption of malachite green on both types of nanoparticles. However,  $R_L$  values for 2 are smaller than 1 which means that adsorption with 2 is more favorable than with 1 [27, 28, 46].

It was also observed that  $K_L$  increases with temperature, indicating that the adsorption of malachite green onto the adsorbents improves with temperature. The results obtained with the Freundlich isotherm also suggest that the values of  $K_F$  increase with temperature. Raising the temperature causes an increase in the mobility of dye molecules and thus an increase in the molecular chance for interacting with the active

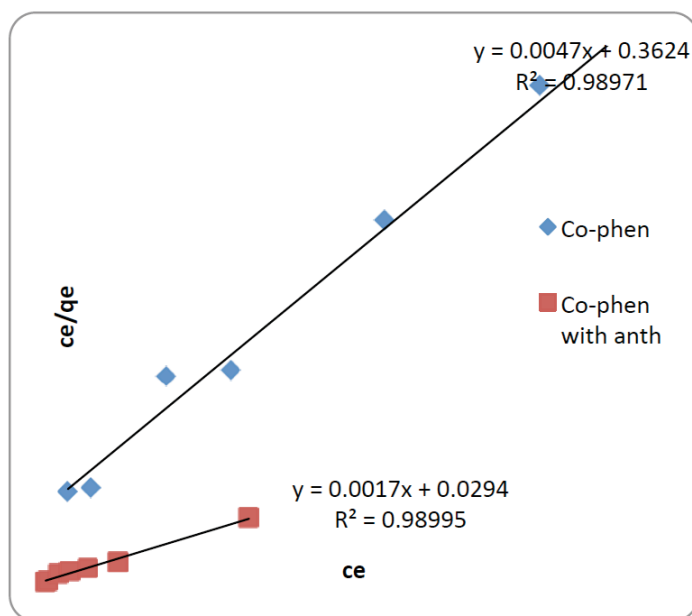


**Fig. (7a).** Langmuir isotherm (linear) at 25°C for adsorption of MG dye onto adsorbents **1** (from pyrolysis of Co-phen (complex)) and **2** (from pyrolysis of Co-phen (complex) with anth (anthracene)).

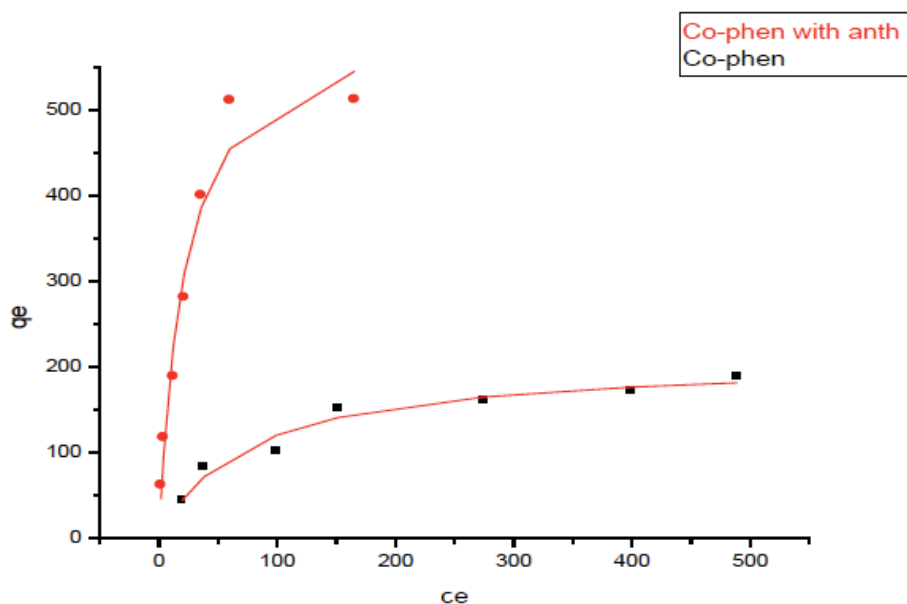


**Fig. (7b).** Langmuir isotherm (non-linear) for adsorption of MG dye onto adsorbents **1** and **2** at 25 °C.

sites on adsorbents. The values of the Freundlich constant (heterogeneity factor)  $n_F = 1/n$  are lower than 1 which points out that adsorption of malachite green onto adsorbents **1** and **2** is favorable [27, 28, 44]. When applying the Temkin isotherm [31, 32, 36] Table 1, adsorption on adsorbent **2** gives higher  $B_T$  values than **1** which can be due to the higher binding energy, Table 9. It was also found that Temkin isotherm binding constant  $K_T$  increases with temperatures for both adsorbents **1** and **2**. The values of free energy of sorption per mole of sorbate  $E$  obtained from Dubinin-Radushkevich isotherm (Tables 1 and 10) reveal that it lies between 8 and 16 kJ/mol [27, 33]. Where  $E$  is equal to  $1/(-2\beta)^{0.5}$ . This indicates

that adsorption of MG onto surfaces of adsorbent **1** and **2** is being controlled by ion exchange.

#### 4.4.5. Adsorption Thermodynamics

The thermodynamic parameters (free energy ( $\Delta G$ ), enthalpy ( $\Delta H$ ), and entropy ( $\Delta S$ )) play an important role in determining the heat change for the adsorption process.  $\Delta H$  and  $\Delta S$  parameters can be obtained from the slope and intercept of the plot  $\ln K_D$  versus  $1/T$ , van't Hoff equations where  $K_D$  is the distribution coefficient [21]. The results are summarized in Table 11. The negative value of  $\Delta G$  indicates that the adsorption process is spontaneous. The decrease in  $\Delta G$

Table 7. Langmuir and Freundlich linear isotherm constants for MG adsorption onto 1 and 2 at different temperatures.

Sample	Temperature (K)	Langmuir Model (linear)				Freundlich Model (linear)		
		$Q^0$ (mg/g)	$K_L$ (L/mg)	$R_L$	$R^2$	$K_F$ (mg/g) $\times$ (L/mg) <sup>1/n</sup>	1/n	$R^2$
(1)	298	212.76	0.013	0.28	0.99	15.53	0.42	0.93
	303	217.39	0.070	0.07	0.99	46.99	0.31	0.91
	308	250.00	0.075	0.06	0.99	47.63	0.29	0.90
	313	270.27	0.113	0.04	0.99	64.68	0.26	0.85
(2)	298	588.23	0.058	0.08	0.99	57.16	0.49	0.95
	303	666.67	0.059	0.08	0.97	73.00	0.68	0.97
	308	769.23	0.062	0.07	0.99	51.20	0.67	0.95
	313	833.33	0.132	0.04	0.99	107.60	0.54	0.95

Table 8. Langmuir and Freundlich non-linear isotherms constants for MG adsorption onto 1 and 2 at different temperatures.

Sample	Temperature (K)	Langmuir Model (Non-linear)			Freundlich Model (Non-linear)		
		$Q^0$ (mg/g)	$K_L$ (L/mg)	$R^2$	$K_F$ (mg/g) $\times$ (L/mg) <sup>1/n</sup>	1/n	$R^2$
(1)	298	200.60	0.014	0.96	21.42	0.36	0.93
	303	210.73	0.042	0.95	64.55	0.2	0.92
	308	235.92	0.065	0.90	67.74	0.19	0.69
	313	265.44	0.119	0.95	80.06	0.17	0.87
(2)	298	492.01	0.031	0.99	56.00	0.52	0.87
	303	615.20	0.045	0.98	80.92	0.44	0.96
	308	769.23	0.047	0.99	95.35	0.42	0.97
	313	833.33	0.130	0.99	145.3	0.35	0.94

with increasing temperature indicates more efficient adsorption at higher temperature. The value of  $\Delta G$  in the case of physical adsorption is in the range -12 to 0 KJ/mol, while for chemical adsorption it is between -400 and -80 kJ/mol [46]. The  $\Delta G$  values obtained at different temperatures are between -20 to 0 KJ/mol suggesting a physical nature of adsorption of MG onto 1 and 2 [35-37, 46]. The positive enthalpy values confirm that the adsorption process is endothermic. When malachite green ions travel through solution and reach the adsorption site, they must be stripped off of their hydration shell, and the process thus consume energy. Furthermore, the positive values of  $\Delta S$  indicate that the de-

grees of freedom increase at the solid-liquid interface during the adsorption of malachite green onto carbon-cobalt nanostructures.

Thus the low values of activation energy  $E_a$  are between 5 and 40 KJ/mol indicate fast physisorption for adsorption of MG onto both adsorbents 1 and 2 surfaces, Table 12 [36, 37, 47], and therefore the interaction between MG and nanostructures involves van der Waals interaction.

The adsorption capacity (mg/g) of MG by adsorbent 2 (492.01) in a batch experiment is higher than other reported carbonaceous adsorbents, such as hydrothermally carbonized

**Table 9.** Temkin linear isotherm constants for MG adsorption onto adsorbent 1 and 2 at different temperatures.

Carbon-Cobalt Nanoparticle (1)	Temperature (K)	Temkin Model (Linear)		
		$K_T$ (L/mg)	$B_T$ (J/mol)	$R^2$
(1)	298	0.15	43.34	0.97
	303	2.14	26.16	0.96
	308	2.32	29.95	0.89
	313	3.21	37.99	0.95
(2)	298	0.85	108.12	0.97
	303	0.86	200.11	0.96
	308	0.84	149.70	0.98
	313	1.39	162.31	0.99

**Table 10.** Temkin and D-R non-linear isotherm constants for MG adsorption onto 1 and 2 at different temperatures.

Sample	Temper-ature (K)	Temkin Model (Non-linear)			D-R Model (Non-linear)			
		$K_T$ (L/mg)	$B$ (J/mol)	$R^2$	$-\beta$ (mol <sup>2</sup> /kJ <sup>2</sup> )	$E$ (kJ/mol)	$Q_m$ (mg/g)	$R^2$
(1)	298	0.15	24.29	0.97	0.014	6.00	186.10	0.93
	303	1.95	29.84	0.95	0.005	10.44	190.60	0.96
	308	2.89	39.84	0.76	0.004	10.80	197.12	0.94
	313	6.03	43.34	0.93	0.002	15.77	257.40	0.89
(2)	298	0.42	112.25	0.93	0.005	10.03	565.76	0.95
	303	0.78	116.72	0.93	0.005	10.30	631.93	0.96
	308	1.06	140.56	0.98	0.005	10.49	640.79	0.97
	313	2.13	149.09	0.96	0.002	16.22	671.11	0.95

pine needles (97.08) [37], waste apricot activated carbon (116.27) [48], and ground nut shell waste activated carbon (222.22) [49].

#### 4.5. Column Adsorption Study

This experiment was carried in order to determine the breakthrough curve and thus to explain the loading behavior of pollutant to be eliminated from waste water in a fixed bed operation.

The experimental data of column adsorption in a fixed bed operation packed with adsorbent 2 was fitted with Thomas, Yoon-Nelson, and Yan model [40-42]. The rate

constants, capacity and  $R^2$  coefficient are presented in Table 3, [28, 34-37].

There is a close agreement between column capacity values  $q_e$  (63.84 mg/g) obtained by the breakthrough curve area method (Table 2) and those predicted by Thomas model  $q_{Th}$  (60.50 mg/g) and Yoon nelson model  $q_{YN}$  (66.67 mg/g). However, there is a large deviation from values obtained by Yan model  $q_Y$  (94.90 mg/g), Table 3. This is also supported by highest  $R^2$  value obtained for the Thomas 0.9757, compared to lowest  $R^2$  value for the Yan model 0.9012, Table 3. This indicates that the column adsorption data is best fitted by Thomas model, Figure 8, consequently the sorption process follows Langmuir kinetics of adsorption-desorption

**Table 11.** Thermodynamic parameters of MG adsorption onto adsorbents 1 and 2, using 0.01 g of adsorbent in 10 ml of 200 ppm MG solution.

Sample	T (°K)	Distribution Coefficient $K_D$ $\pm 0.01$	Enthalpy $\Delta H$ (kJ/mol) $\pm 0.05$	Entropy $\Delta S$ (J/mol.K) $\pm 0.1$	Gibbs Free Energy Change $\Delta G$ (kJ/mol) $\pm 0.05$	
(1)	298	1.03	109.39	367.61	298	-0.16
	303	2.21			303	-2.00
	308	5.57			308	-3.83
	313	7.90			313	-5.67
(2)	298	15.55	86.24	311.11	298	-6.47
	303	19.17			303	-8.03
	308	45.55			308	-9.59
	313	74.64			313	-11.14

**Table 12.** Thermodynamic Activation parameters of malachite green adsorption onto adsorbent 1 and 2 using 0.01 g of adsorbent in 10 ml of 200 ppm MG solution.

Sample	Temperature (°K)	Rate Constant $k_1$ (h <sup>-1</sup> ) $\pm 0.01$	Enthalpy $\Delta H^\ddagger$ (kJ/mol) $\pm 0.05$	Entropy $\Delta S^\ddagger$ (kJ/mol K) $\pm 0.1$	Gibbs Free Energy $\Delta G^\ddagger$ (kJ/mol) $\pm 0.1$	Activation Energy $E_a^\ddagger$ (kJ/mol) $\pm 0.05$
(1)	298	1.04	5.01	-0.30	93.19	7.55
	303	1.07			94.66	
	308	1.13			96.15	
	313	1.20			97.63	
(2)	298	0.26	18.43	-0.26	96.64	20.97
	303	0.29			97.95	
	308	0.33			99.26	
	313	0.38			100.57	

with no axial dispersion [36] and the rate determining process obeys second-order reversible reaction kinetics. The highest breakthrough time for 50 % removal predicted by Yoon-Nelson model  $\tau_{YN}$  is equal to 90.83 min.

The removal of dye (column performance) in % and the column capacity  $q_e$  calculated for three consecutive cycles drops slightly in the order 54.36,  $\rightarrow$  53.69, 47.38%, and 63.84, 45.32, 42.27 mg/g respectively, suggesting that the adsorbent materials are stable during uptake and regeneration experiments, Table 2. The remaining equilibrium concentrations  $C_e$  increases from 83.75, 84.96, to 97.27 mg/L. Therefore, by regeneration of the column efficient reuse of the packed adsorbent 2 for multiple cycles of application was achieved and thus the treatment cost can be minimized.

## CONCLUSION

Preparation of carbon-cobalt nanostructure adsorbents 1 and 2 involves single-step pyrolysis of complex 3, cis-[Co(phen)<sub>2</sub>Cl<sub>2</sub>].1.5 acetonitrile, in absence or presence of anthracene carbon source, respectively. Bonds distances, complexation energies, and relative energies of the complex cis-[Co(phen)<sub>2</sub>Cl<sub>2</sub>] in different spin states were evaluated by DFT calculation. FE-SEM analysis of 1 and 2 indicates the presence of 3D nanostructure hierarchical porous graphitic carbons HPCGs with mesopores and macropores ranging from 20-100 nm, as well as cobalt spheres and rods. TEM analysis of adsorbents 1 and 2 indicates that their structures are heterogeneous consisting of cobalt nanoparticles, gra-

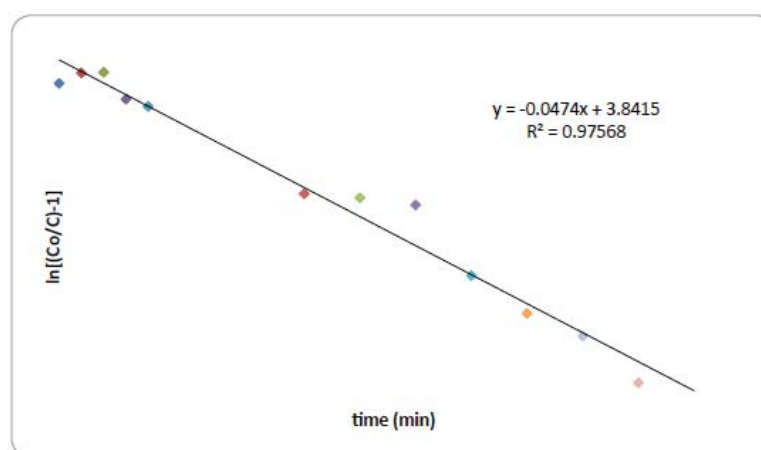


**Fig. (8).** Thomas model for MG adsorption onto 2..

phitic layers and graphitic hollow nanostructures (SWCNT and MWCNT).

A pseudo-first order model describes best the kinetic adsorption process of Malachite Green MG for both adsorbents. The adsorption data was best fitted by a Langmuir isotherm model. The adsorption capacity of **2** (492 mg/g) was greater than **1** (200 mg/g) and superior to other reported adsorbents. Thermodynamics indicates that adsorption is spontaneous, endothermic, entropically controlled, and follows a physisorption process.

Column adsorption data of MG by adsorbent **2** was described by Thomas model with a capacity of 63.84 mg/g, and relatively unchanged for three consecutive cycles. Thus **2** can be used as a potential adsorbent in water treatment for removal of cationic organic pollutants.

#### ETHICS APPROVAL AND CONSENT TO PARTICIPATE

Not applicable.

#### HUMAN AND ANIMAL RIGHTS

No Animals/Humans were used for studies that are base of this research.

#### CONSENT FOR PUBLICATION

Not applicable.

#### CONFLICT OF INTEREST

The authors declare no conflict of interest, financial or otherwise.

#### ACKNOWLEDGEMENTS

Dr Volker Enkelmann and Mohamad A. Mawass are acknowledged for performing single crystal X-ray analysis. Dr Syed Ghazanfar Hussain at KFU is also acknowledged for performing FE-SEM analysis.

#### SUPPLEMENTARY MATERIAL

Supplementary material is available on the publishers Web site along with the published article.

#### REFERENCES

- [1] V. G. Pol, S. V. Pol, A. Gedanken, V. G. Kessler, G. A. Seisenbaeva, M.-G. Sung, S. Asai, Applied Magnetic Field Rejects the Coating of Ferromagnetic Carbon from the Surface of Ferromagnetic Cobalt: RAPET of  $\text{CoZr}_2(\text{acac})_2(\text{O}-i\text{-Pr})_8$ , *J. Phys. Chem. B.* 2005, 109 (13), 6121-6125.
- [2] A.-H. Lu, W. Schmidt, N. Matoussevitch, H. Bönemann, B. Spliethoff, B. Tesche, E. Bill, W. Kiefer and F. Schüth, Nanoengineering of a magnetically separable hydrogenation catalyst, *Angew.Chem. Int. Ed.* 2004, 43, 4303-4306.
- [3] J. Jiao, S. Seraphin, X. Wang, J. C. Withers, Preparation and properties of ferromagnetic carbon-coated Fe, Co, and Ni nanoparticles, *J. Appl. Phys.* 1996, 80, 103-108.
- [4] A.H. Lu, W. C. Li, N. Matoussevitch, B. Spliethoff, H. Bönemann, F. Schüth, Highly stable carbon-protected cobalt nanoparticles and graphite shells, *Chem. Commun.* 2005, 1, 98-100.
- [5] V. S. Iyer, K. P. C. Vollhardt, R. Wilhelm, Near-Quantitative Solid-State Synthesis of Carbon Nanotubes from Homogeneous Diphenylethynecobalt and -Nickel Complexes, *Angew. Chem. Int. Ed.* 2003, 42, 4379-4383
- [6] S. Scholz, P. J. Leech, B. C. Englert, W. Sommer, M. Weck, U. H. F. Bunz, Cobalt-carbon spheres: Pyrolysis of dicobalthexacarbonyl-functionalized poly(p-phenyleneethynylene)s, *Adv. Mater.* 2005, 17, 1052-1056.
- [7] S. J. Teng, J. N. Wang, B. Y. Xia, X. X. Wang, A General Strategy for the Preparation of Hollow Carbon Nanocages by  $\text{NH}_4\text{Cl}$ -Assisted Low-Temperature Heat Treatment, *Chem. Eur. J.* 2010, 16, 13603 – 13608.
- [8] Leonhardt, M. Ritschel, D. Elefant, N. Mattern, K. Biedermann, S. Hampel, C. Muller, T. Gemming, B. Buchner, Enhanced magnetism in Fe-filled carbon nanotubes produced by pyrolysis of ferrocene, *J. Appl. Phys.* 2005, 98, 074315.
- [9] M. Sevilla, C. Salinas Martínez-de Lecea, T. Valdes-Solis, E. Morallon and A. B. Fuertes, Solid-phase synthesis of graphitic carbon nanostructures from iron and cobalt gluconates and their utilization as electrocatalyst supports, *Phys. Chem. Chem. Phys.*, 2008, 10, 1433-1442
- [10] E. Hamaoui, L. Zhi, J. Wu, U. Kolb, K. Müllen, Uniform Carbon and Carbon/Cobalt Nanostructures by Solid-State Thermolysis of Polyphenylene Dendrimer/Cobalt Complexes, *Adv. Mater.* 2005, 17, 2957-2960.
- [11] M. Laskoski, W. Steffen, J. G. M. Morton, M. D. Smith, U. H. F. Bunz, Synthesis and Explosive Decomposition of Organometallic Dehydro[18]annulenes: An Access to Carbon Nanostructures, *J. Am. Chem. Soc.* 2002, 124, 13 814-13818.
- [12] L. J. Zhi, T. Gorelik, R. Friedlein, J. S. Wu, U. Kolb, W. R. Salaneck, K. Mullen, Solid-State Pyrolyses of Metal Phthalocyanines: A Simple Approach towards Nitrogen-Doped CNTs and Metal Core/Carbon Sheath Nanocables, *Small*, 2005, 1, 798-801.
- [13] . Wu, B. E. Hamaoui, J. Li, L. Zhi, U. Kolb, and K. Mullen, Solid-State Synthesis of "Bamboo-Like" and Straight Carbon Nanotubes

- by Thermolysis of Hexa-peri-hexabenzocoronene-Cobalt Complexes, *Small*, 2005, 1 (2), 210–212
- [14] L. Chen, J. Bai, C. Wang, Y. Pan, M. Scheerc, X. Youa, One-step solid-state thermolysis of a metal-organic framework: a simple and facile route to large-scale of multiwalled carbon nanotubes, *Chem. Commun.*, 2008, 1581–1583
- [15] E. Hamaoui, L. Zhi, J. Wu, J. Li, N. T. Lucas, Z. Tomovic', U. Kolb, and K. Müllen, Solid-State Pyrolysis of Polyphenylene-Metal Complexes: A Facile Approach Toward Carbon Nanoparticles, *Adv. Funct. Mater.* 2007, 17, 1179–1187
- [16] Shrivastava, S., Sinha, R. and Roy, D. Toxicological effects of malachite green, *Aquatic Toxicology*, 2004, 66 (3), 319-329.
- [17] Venkata K. K. Upadhyayula, Shuguang. Deng, Martha C. Mitchell, Geoffrey B. Smith Application of carbon nanotube technology for removal of contaminants in drinking water, *Science of the Total Environment*, 2009, 408, 1-13.
- [18] Fei Yu, Yanqing Wu, Jie Ma, Chi Zhang, Adsorption of lead on multi-walled carbon nanotubes with different outer diameters and oxygen contents: Kinetics, isotherms and thermodynamics, *Journal of Environmental Sciences*, 2013, 25, 195.
- [19] Hyeong Taek Ham, Chong Min Koo, Sang Ouk Kim, Yeong Suk Choi, and In Jae Chung, Chemical Modification of Carbon Nanotubes and Preparation of Polystyrene/Carbon Nanotubes Composites, *Macromolecular Research*, 2004, 12 (4), 384.
- [20] Chao-Yin Kuo, Han-Yu Lin, Adsorption of aqueous cadmium (II) onto modified multi-walled carbon nanotubes following microwave/chemical treatment, *Desalination*, 2009, 249, 792.
- [21] Zohre Shahryari, Ataallah Soltani Goharri and Mehdi Azadi, Experimental study of methylene blue adsorption from aqueous solutions onto carbon nanotubes, *Int. J. Water Res. Environ. Eng.*, 2010, 2, 16.
- [22] Dai, H. Carbon nanotubes: Synthesis, integration, and properties. *Acc. Chem. Res.* 2002, 35, 1035.
- [23] a) A. Hazell, J. McGinley, C. J. McKenzie, Dichlorobis(1,10-phenanthroline-N,N')-cobalt(II)-Acetonitrile (1/1.5), *Acta Cryst.* 1997, C53, 723-725. b) S.-L. Cai, S.-M. Ying, H. Li, Y. Chen, cis-Dichloro-bis(1,10-phenanthroline)-cobalt(II) dimethylformamide solvate, *Acta Crystallogr., Sect. E: Struct. Rep. Online*, 2008, 64, m1328.
- [24] a) A M. J. Frisch, G. W. Trucks, H. B. Schlegel, G. E. Scuseria, M. A. Robb, J. R. Cheeseman, G. Scalmani, V. Barone, B. Mennucci, G. A. Petersson, H. Nakatsuji, M. Caricato, X. Li, H. P. Hratchian, A. F. Izmaylov, J. Bloino, G. Zheng, J. L. Sonnenberg, M. Had and DJF (2010) Gaussian 09, Rev C.01, Gaussian Inc. b) Kruse H, Goerigk L, Grimme S (2012) Why the standard B3LYP/6-31G\* model chemistry should not be used in DFT calculations of molecular thermochemistry: Understanding and correcting the problem. *J Org Chem* 77:10824–10834.
- [25] C. N. R. Rao, A. Govindaraj, Carbon nanotubes from organometallic precursor, *Acc. Chem. Res.* 2002, 35, 998. b) Fangwei Ma, Di Ma, Guang Wu, Weidan Geng, Jinqiu Shao, Shijiao Song, Jiafeng Wan and Jieshan Qiu, *Chem. Commun.* 2016, 52, 6673–6676
- [26] H. H. Hammud, M. E. Mansour, S. Shaalan, E. Khamis, A. El-Shaar, Adsorption of Mercuric Ion by Marine Algae *Enteromorpha*, *Int. J. Appl. Chem.* 2006, 2(2), 87-102.
- [27] H. H. Hammud, L. Fayoumi, H. Holail, El-S. M. E. Mostafa, Biosorption studies of methylene blue by Mediterranean algae *Carolina* and its chemically modified forms Linear and nonlinear models' prediction based on statistical error calculation, *International J. chemistry*, 2011, 3(4), 147-163.
- [28] H. H. Hammud, M. M. Chahine, B. El Hamaoui and Y. Hanifehpour, Lead uptake by new silica-carbon nanoparticles, *European Journal of Chemistry*, 2013, 4 (4), 432-440.
- [29] Purkait, M.K.; Gusain, D.S.; Das Gupta, S.; De, S., Adsorption behavior of chrysoidine dye on activated charcoal and its regeneration characteristics using different surfactants, *Sep. Sci. and Technol.*, 2004, 39 (10), 2419–2440.
- [30] Ho., Y. S.; McKay, G.; Pseudo-second order model for sorption processes, *Process Biochem.* 1999, 34 (5), 451–465.
- [31] G. P. Jeppu, T. P. Clement, A modified Langmuir-Freundlich isotherm model for simulating pH-dependent adsorption effects, *Journal of Contaminant Hydrology*, 2012, 129–130, 46.
- [32] M. Vadi, M. Abbasi, M. Zakeri, B. J. Yazdi, Application of the Freundlich, Langmuir, Temkin and Harkins-Jura Adsorption Isotherms for Some Amino Acids and Amino Acids Complexation with Manganese Ion(II) on Carbon Nanotube, *J. Phys. Theor. Chem.* 2010, 7, 95.
- [33] Ido A.U. and Ido H.U, Sorption Energies Estimation Using Dubinin-Radushkevich and Temkin Adsorption Isotherms, *Life Science Journal*, 2010, 7, 68.
- [34] Hassan H. Hammud, Ali El-Shaar, Essam Khamis, and El-Sayed Mansour, Adsorption Studies of Lead by *Enteromorpha* Algae and Its Silicates Bonded Material. *Advances in Chemistry*, Volume 2014, 11 pages. <http://dx.doi.org/10.1155/2014/205459>
- [35] Hassan H. Hammud, Ismail Abbas and Diana Al-khalili, Kinetics and Thermodynamics of Chromate and Phosphate Uptake by Polypyrrole: Batch and Column Studies, *J. Inclusion Phenomena and Macrocyclic Chemistry*, 2015, 82, 395–405.
- [36] Mohammad Hanbali, Hanafy Holail, Hassan Hammud, Remediation of lead by pretreated red algae: adsorption isotherm, kinetic, column modeling and simulation studies, *Green Chemistry Letters and Reviews*, 2014, 7 (4), 342–358.
- [37] Hassan Hammud, Abeer Shmait, Nadim Hourani, Removal of Malachite Green from Water using Hydrothermally Carbonized Pine Needles, *RSC Advances*, 2015, 5, 7909-7920.
- [38] Chu, K.H., Improved fixed bed models for metal biosorption, *Chemical Engineering Journal*, 2004, 97, 233-239.
- [39] Malkoc, E.; Nuhoglu, Y.; Removal of Ni(II) ions from aqueous solutions using waste of tea factory: adsorption on a fixed bed column, *Journal of Hazardous Materials*, 2006, B135, 328-336.
- [40] J.R. Rao, T. Viraraghavan, Biosorption of phenol from an aqueous solution by *Aspergillus niger* biomass, *Bioresource Technol.* 2002, 85,165-171.
- [41] Y. H. Yoon, J. H. Nelson, Application of gas adsorption kinetics. I. A theoretical model for respirator cartridge service life, *Am. Ind. Hyg. Assoc. J.* 1984, 45, 509-516.
- [42] G. Y. Yan, T. Viraraghavan, M. Chen, A new model for heavy metal removal in a biosorption column, *Adsorp. Sci. Tech.* 2001, 19, 25-43.
- [43] Nose H, Chen Y, Rodgers MT, Energy-resolved collision-induced dissociation studies of 1,10-phenanthroline complexes of the late first-row divalent transition metal cations: Determination of the third sequential binding energies. *J Phys Chem A*, 2013, 117:4316–4330. doi: 10.1021/jp401711c
- [44] Chung-Hsin Wu, Adsorption of reactive dye onto carbon nanotubes: Equilibrium, kinetics and thermodynamics, *Journal of Hazardous Materials*, 2007, 144(1-2), 93.
- [45] Ola Abed El Wahab, Ahmed El Nemr, Amani El Sikaily, Azza Khaled, Use of rice husk for adsorption direct dye from aqueous solution, *Egyptian Journal of Aquatic Research*, 2005, 31, 1.
- [46] Zhengang Liu and Fu-Shen Zhang, Removal of lead from water using biochars prepared from hydrothermal liquefaction of biomass, *Journal of Hazardous Materials*, 2009, 167, 933.
- [47] Hardiljeet K. Boparai, Meera Joseph and Denis M. O'Carroll, Kinetics and Thermodynamics of Cadmium Ion Removal by Adsorption onto Nanozero Valent Iron Particles, *Journal of hazardous material*, 2011, 186, 458.
- [48] Basar, Applicability of the various adsorption models of three dyes adsorption onto activated carbon prepared apricot, *J. Hazard. Mater.*, 2006, 135, 232–241.
- [49] R. Malik, D. S. Ramteke and S. R. Wate, Adsorption of Malachite Green on groundnut shell waste based powdered activated carbon, *Waste Management*, 2007, 27, 1129–1138.

DISCLAIMER: The above article has been published in Epub (ahead of print) on the basis of the materials provided by the author. The Editorial Department reserves the right to make minor modifications for further improvement of the manuscript.